Charge transfer equilibria in ambient-exposed epitaxial graphene on $(000\bar{1})$ 6 H-SiC

Anton N. Sidorov,[1] Kurt Gaskill,[2] Marco Buongiorno Nardelli,[3,4] Joseph L. Tedesco,[2] Rachel L. Myers-Ward,[2] Charles R. Eddy Jr.,[2] Thushari Jayasekera,[3] Ki Wook Kim,[5] Ruwantha Jayasingha,[6] Andriy Sherehiy,[6] Robert Stallard,[6] and Gamini U. Sumanasekera[6]
[1]*School of Physics, Georgia Institute of Technology, Atlanta, Georgia 30332, USA*
[2]*Advanced SiC Epitaxial Research Laboratory, U.S. Naval Research Laboratory, Washington, DC 20375, USA*
[3]*Computer Science and Mathematics Division, Oak Ridge National Laboratory, Oak Ridge, Tennessee 37831-6359, USA*
[4]*Department of Physics and Department of Chemistry, University of North Texas, Denton, Texas 76203, USA*
[5]*Department of Physics, North Carolina State University, Raleigh, North Carolina 27695-7518, USA*
[6]*Department of Physics & Astronomy, University of Louisville, Louisville, Kentucky 40292, USA*

(Received 5 January 2012; accepted 3 May 2012; published online 5 June 2012; corrected 25 June 2012)

The transport properties of electronic materials have been long interpreted independently from both the underlying bulk-like behavior of the substrate or the influence of ambient gases. This is no longer the case for ultra-thin graphene whose properties are dominated by the interfaces between the active material and its surroundings. Here, we show that the graphene interactions with its environments are critical for the electrostatic and electrochemical equilibrium of the active device layers and their transport properties. Based on the prototypical case of epitaxial graphene on $(000\bar{1})$ 6 H-SiC and using a combination of *in-situ* thermoelectric power and resistance measurements and simulations from first principles, we demonstrate that the cooperative occurrence of an electrochemically mediated charge transfer from the graphene to air, combined with the peculiar electronic structure of the graphene/SiC interface, explains the wide variation of measured conductivity and charge carrier type found in prior reports. © *2012 American Institute of Physics*. [http://dx.doi.org/10.1063/1.4725413]

I. INTRODUCTION

The exposure of graphene samples to different gases has been shown to selectively induce p- and n-type behavior in the intrinsic case (suspended graphene electronically decoupled from the substrate).[1–5] Although exfoliated graphene has been demonstrated as an ideal platform for proof-of-concept research,[6–8] epitaxial graphene is the practical production route for electronics applications due to compatibility with wafer-scale processing techniques.[3,9–11] The epitaxial system is characterized by an additional layer of complexity in the fact that the graphene now interacts not only with the ambient but also with the underlying substrate. A comprehensive analysis of the electronic and transport properties of this material in this complex environment is of paramount importance.

II. EXPERIMENTAL SETUP

Epitaxial graphene is produced via the thermal decomposition of either 4 H- or 6 H-SiC. Samples are typically several layers thick on C-terminated surfaces (multilayer epitaxial graphene, MEG) and one to two layers thick on Si-terminated surfaces.[12–14] The geometry of the graphene/SiC interface and the bonding that takes place in this region play a dominant role in the determination of the electronic properties of the active graphene layers: interface modifications can lead to a fine-tuning of the doping and band alignment of the system and provide a clear insight into the mechanisms of charge transfer and interface stability.[15] These findings, when placed in the more general context of ambient exposed graphene samples, provide the framework for the interpretation of the experimental results and a generalization to a universal behavior that should be expected in many other common situations.

The goal of our study is to provide a quantitative and systematic evaluation of the impact of ambient exposure in epitaxial graphene samples. To this aim, we performed simultaneous thermo-electric power (TEP) and resistance (R) measurements on multi- and 1- to 3-layer epitaxial graphene samples[14] that were placed in a quartz reactor which has provisions for evacuation and exposure to various gasses at desired temperatures and pressures. The 4×4 mm^2 multilayer epitaxial graphene/SiC samples were mounted on a ceramic holder attached to a probe as shown on Figure 1. The probe is loaded into a quartz reactor placed inside a tube furnace. Two Chromel/Alumel thermocouples $\sim 100\,\mu$m in diameter were mounted on the sample with silver epoxy and a small heater was placed on one end of the sample. For four-probe resistance measurements, two extra copper wires are attached as current leads. The reactor is evacuated to 2×10^{-7} a base pressure below 10^{-6} Torr using a turbo molecular pump and degassed at 500 K, while the time evolution of the Seebeck coefficient and the four-point resistance are recorded concomitantly. Then the reactor is cooled down to room temperature under high vacuum. To measure the Seebeck coefficient, a temperature difference ($\Delta T \approx 1$ K) is generated across the sample by applying a voltage pulse to the heater. The typical heating power is ~ 10 mW, and the pulse

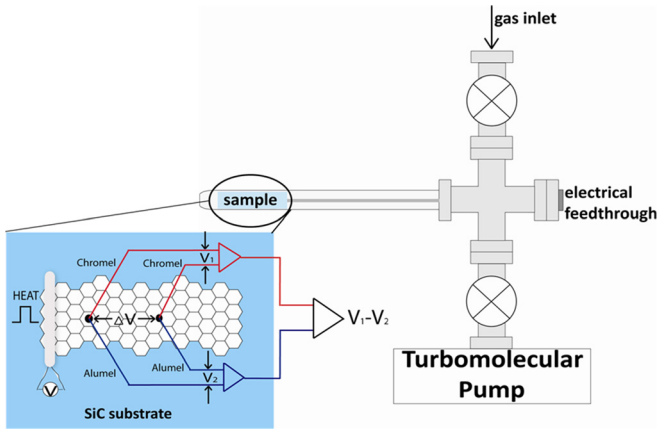

FIG. 1. The schematics of the TEP measurement system. (a) Schematic diagram of the quartz reactor containing the sample located inside a tube furnace and connected to a turbo molecular pump and a gas handling system. (b) Graphene sample with two K-type thermocouples attached ~2 mm apart with a platinum resistive heater anchored closer to one thermocouple. Voltages V_1, V_2, and $\Delta V = V_1 - V_2$ used to determine the thermo-emf (ΔV) and the temperature difference (ΔT) are also shown.

duration is 3–5 seconds.To measure TEP, a temperature difference ΔT is introduced across the sample by applying a voltage pulse across a platinum resistive heater, as shown in Figure S1. The slope of the thermo-emf (ΔV) versus temperature difference (ΔT) due to the heat pulse is used to obtain TEP at a given temperature. In order to measure the 4-probe resistance (R), an excitation current was applied through the two current leads and the voltage across the two thermocouple wires was measured. Further experimental details are described in Ref. 14. The TEP and R of graphene were measured over a temperature range of 300 K to 550 K.

The sign of the TEP provides information about changes in the doping type of the active graphene layers and, in particular, of the relative energetic position of the Fermi level, E_F, and the Dirac point energy, E_D (the energy of the vertex of the Dirac cone), due to exposure to the ambient: a positive TEP is the signature of a p-type (electron depletion) doping, while a negative TEP corresponds to n-type doping (electron addition). Conversely, the resistance R of the sample correlates with the density of the charge carriers available for transport on the active layer.

III. RESULTS AND DISCUSSION

In the initial experiment, we prepared an as-grown MEG sample on C-face SiC and starting from ambient conditions, we measured the variation of the thermo-electric response as a function of the environment composition. The results, displayed in Figures 2(a)–2(c), show that initially the system possesses a p-type doping character with a TEP value of $S \sim +10\ \mu V/K$ and $R \sim 7\ \Omega$. The sample was then annealed at 500 K under high vacuum conditions ($P = 2 \times 10^{-7}$ Torr). Interestingly, the TEP changed sign (an indication that the sample becomes n-type) to finally reach a constant value of $S \sim -20\ \mu V/K$. As the sample was cooled back to 300 K under vacuum, the TEP became even more negative and eventually saturated at $\sim -30\ \mu V/K$. As seen in Figure 2(b), the resistance R of the sample increased from its room temperature value of $\sim 7\ \Omega$ to reach $\sim 10\ \Omega$ under vacuum at 500 K and eventually saturated at $\sim 8\ \Omega$ During cooling, R continued to decrease, returning to its initial value of $\sim 7\ \Omega$. These findings are clearly interpreted in terms of the interplay between TEP and resistance: Figure 2(c) demonstrates that as TEP approaches zero, the resistance increases and reaches its maximum value when the TEP signal changes sign. This is an indication that the sheet charge density is decreasing upon annealing and becomes zero when the TEP is zero. This corresponds to passing through the Dirac Point, where indeed the resistance achieves its expected maximum value. After this point, the graphene becomes n-type and eventually reaches its intrinsic conductivity value.

In order to ascertain the reproducibility of these results and confirm that the variation between n- and p-type conductivity was a result of factors from the environment, we re-exposed the above sample to the ambient. Indeed the TEP measurement gave again a value of $S > 0$, that is, the graphene was p-type. Repeating the vacuum annealing process restored n-type doping with $S \sim -30\ \mu V/K$, showing the reproducibility of our measurements. Finally, in order to rule out possible effects of the surface preparation, we repeated the measurements on a sample that was first vacuum annealed at elevated temperatures to prepare a pristine graphene surface. Then the ambient was introduced into the vacuum system at room temperature. The initially negative TEP signal ($\sim -30\ \mu V/K$) of the annealed graphene gradually increased, passed through zero, and reached a positive

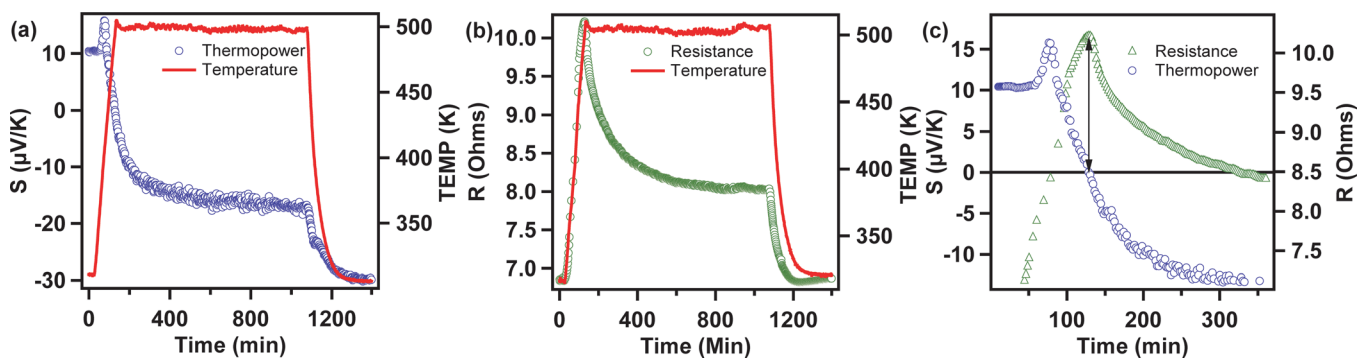

FIG. 2. Simultaneous TEP and R measurements of multilayer epitaxial graphene (MEG) on C-face SiC. The time evolution of the (a) TEP (left axis) and the corresponding temperature profile (right axis) are plotted during the vacuum-annealing process. (b) Simultaneous behavior of R and temperature during the degassing process. (c) Simultaneous TEP and R of the vacuum-annealed MEG on C-face SiC during annealing plotted in an expanded scale.

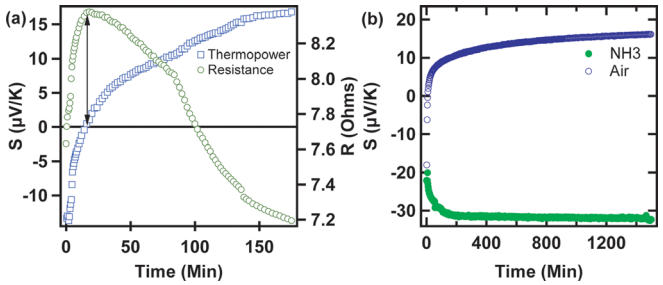

FIG. 3. Simultaneous measurement of TEP and R of the annealed MEG upon (a) exposure to ambient air at 300 K plotted in an expanded scale. (b) exposure to ambient air and ammonia.

value (+15 μV/K) within ~3 h. Concomitantly, the value of R initially increased and passed through a maximum when TEP passed through zero, as expected. These results are summarized in Figure 3(a) and strongly suggest that environmental factors are the cause of the p-type behavior of ambient exposed C-face epitaxial graphene. Without the influence of the ambient, the natural conductivity state of MEG is n-type (Figure 3(b)), as previously reported.[12]

The results above were for a multilayer epitaxial graphene sample; MEG is known to have many layers that could result in competing parallel conductivity paths, clouding the interpretation of the thermopower measurements. Moreover, the typically rough morphology of MEG may increase ambient interaction. To rule out competing effects and isolate completely, the role of the ambient interactions, we performed TEP measurements on single layer graphene produced by the electro static deposition (ESD) technique.[16,17] This technique allows us to controllably remove the top layers in MEG samples and leave only a monolayer of graphene on top of the SiC substrate.[14]

The 1-3 layers of C-face graphene sample were vacuum annealed under the same conditions described above for MEG. As reported in Figure 4, we again found that the TEP under ambient conditions was positive (~+2 μV/K), became negative (~−3 μV/K) after vacuum annealing at ~525 K and became more negative upon cooling to ~300 K. Just as in the MEG case, the exposure of epitaxial graphene to the ambient gave rise to p-type conductivity. The TEP values in both conditions were about an order of magnitude smaller than those in MEG. Since S is proportional to the sheet carrier density, n_s, this implies that the latter is about one order of magnitude lower than the MEG samples, both before and after annealing. It seems likely that the reduced number of layers in the sample is at least partly responsible for the large reduction in sheet carrier density. Indeed, the n-type conductivity of the after anneal result is consistent with the recent interpretation put forward by Lin *et al*., who, analyzing Hall conductivity data in MEG samples, drew the conclusion that the layer(s) closest to the SiC substrate were n-type doped with a carrier concentration of 10^{11} to 10^{12} cm^{-2}, which is about one order of magnitude lower than typical MEG data.[18]

The impact of adsorbates and ambient gases on the electronic properties of graphene systems has been extensively studied. Lohmann *et al*. using gated Hall effect measurements on single layer *exfoliated* graphene concluded that "adsorbed dipolar molecules such as water" resulted in p-type conductivity.[19] More recently, Levesque *et al*. identified the water/oxygen redox couple as the underlying mechanism responsible for charge doping in graphene-SiO_2 and graphene-parylene FETs.[20] However, in the latter work, the choice of the geometry of the sample was chosen in order to preclude strong bonding from playing an important role in the measurement so as to isolate the effect of gas interaction. This is fundamentally different from the epitaxial graphene case, where the interaction with the substrate is not only inevitable, but plays an integral part in the determination of the properties of the active layer. Our thermopower results can only be understood by considering the doping effect of ambient factors combined with the effect of the reconstruction of the 6 H-SiC-graphene interface.

It is by now well established that the exposure of surfaces to air can result in an electrochemically-mediated electron transfer between the system and oxygen contained in the ambient gas (water/oxygen redox couple). This mechanism was originally proposed to explain p-type conductivity characteristics of hydrogen-terminated diamond surfaces[21–24] and has been observed in a variety of other systems (single-wall nanotubes, multi-wall nanotubes and activated carbon fibers) when the band lineup between the ambient and electronic states in the semiconductor is appropriate.[25]

Here, however, the above mechanism is competing with the bonding characteristics of the graphene-SiC interface, which controls the electrostatic and electrochemical boundary conditions for the system. The most evident signature of this interface phase is the presence of a surface state localized on the C rest atoms of the $(2 \times 2)_C$ surface reconstruction of $(000\bar{1})$ of 6 H-SiC. This is the state that pins the Fermi energy of the graphene and makes it n-type in the absence of the charge transfer from the water-oxygen redox couple.[14] Using simulations from first principles based on

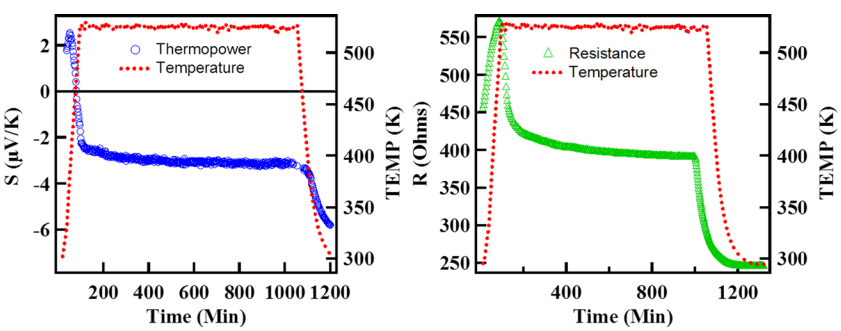

FIG. 4. The time evolution of TEP and R the corresponding temperature profile during the vacuum annealing of the few layers of graphene (1-3 layers) on C-face SiC. The temperature profile is shown on the right axis. The observed behavior is similar to what was observed for the MEG sample shown in Figure 1. Note that the TEP measurement on few layers of C-face graphene is performed on the same sample that had been previously used for TEP measurement of MEG.

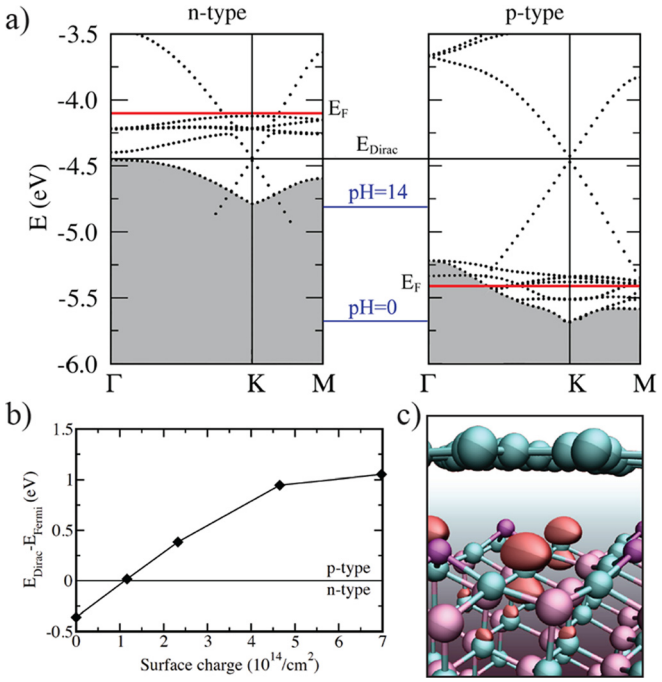

FIG. 5. Energy level diagram of the water/oxygen redox couple (blue lines) compared to the theoretical band diagrams of epitaxial graphene/SiC from our simulations (the zero of energy corresponds to the vacuum level of the system). Shaded areas are the projected bulk bands from the SiC substrate. (a) (left panel) Water-free surface: the E_F is pinned by an interface state located in the conduction band just above the Dirac point causing electron doping of graphene. These states are due to dangling bonds of the C rest atom on the SiC $(000\bar{1})$ $(2\times2)_C$ surface reconstruction (see panel c) and Supplemental Information). (right panel) P-type doping of graphene when the Fermi energy, E_F, is pinned at the chemical potential μ determined by the redox potential of oxygen dissolved in the mildly acidic water adsorbed on the SiC surface. Bands calculated for a (positive) surface charge corresponding to a depletion of $\sim4.5\times10^{14}$ electrons/cm^2. (b) Difference between the Fermi and Dirac energy as a function of surface charge. The neutrality point ($E_{Dirac}=E_{Fermi}$) coincides with a charge depletion of $\sim1\times10^{14}$ electrons/cm^2. (c) Geometry of the graphene/SiC interface (Si, purple; C, cyan; Si adatoms, darker purple). For a detailed account of the interface structure see Supplemental Information. The electron density of the dangling bond state localized on the interface C rest atoms at the Dirac point is shown with the red isosurface (0.15×10^{-3} electrons.)

density functional theory,[14] we have interpreted the results of TEP and R measurements in terms of the interplay between bonding and electrochemical reactions at the surface and demonstrate that indeed, doping from the ambient is a significant contributory factor to the variations in sheet densities.[1,14,17]

In Figure 5(a), we show the energy level diagram of the water/oxygen redox couple (blue lines) compared to the theoretical band diagrams of epitaxial graphene/SiC, as obtained in our first principles simulations. The Fermi energy, ε_F, and the electron chemical potential, μ_{e^-}, are conceptually identical concepts. Usually, ε_F is reported in electron volts per electron referred to the vacuum level. In electrochemistry μ_{e^-} is referred to a potential reference state, often, but not always, the potential, E, of the standard hydrogen electrode (SHE). Thin water films are often present on surfaces exposed to humid air.[13] Within the water film, the dissolved CO_2 gives rise to acidity through the reaction,

$$CO_2 + H_2O = HCO^-_{3(aq)} + H^+_{(aq)}. \quad (1)$$

In turn, the dissolved oxygen and the protons permit the electrochemical redox couple, which in equilibrium fixes the electron chemical potential (Fermi energy) in the film.

$$O_2 + 4H^+_{(aq)} + 4e^- = 2H_2O. \quad (2)$$

If the redox couple and the semiconductor reach equilibrium, their Fermi energies will be equal. Since the water film is in contact with essentially infinite sources of O_2 and CO_2, the Fermi energy will be "pinned" at the electron electrochemical potential of the redox couple. The Fermi energy of the redox couple is given by the Nernst equation, which for Reaction 2 reduces to,

$$\mu_e(eV) = -4.44 + (-1)(+1.23) + \frac{0.0592}{4}[4pH - \log_{10}(p_{O_2})]. \quad (3)$$

In Equation (3), μ_e (eV) is referred to the vacuum level, T = 298 K, the activity of H_2O is taken to be unity, ideal gas behavior is assumed, and P_{O_2} is in bar.

The direction of electron transfer between semiconductor and the redox couple depends on the value of μ_e in both. When the electron chemical potential in the semiconductor is higher than the water film, then electron transfer from the semiconductor to the redox couple, thereby driving Reaction 2 in the forward direction. This results in the formation of a positive space charge layer in the semiconductor and charge-compensating anions in the adsorbed film. At moderate pH, if the semiconductor is exposed to ambient air containing

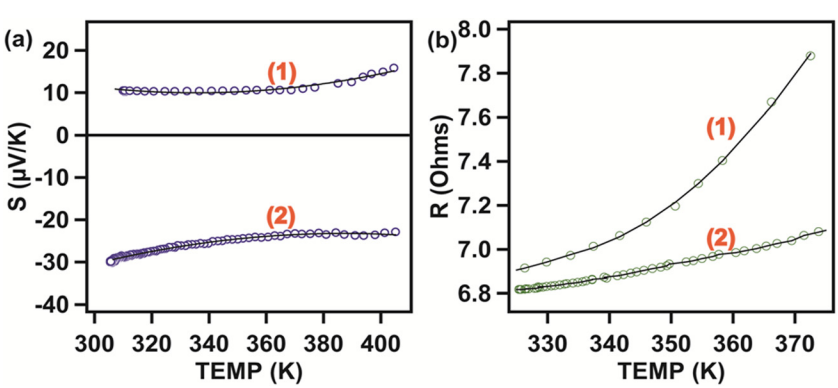

FIG. 6. Temperature dependence of (a) S and (b) R of the vacuum-annealed and air-exposed multilayer epitaxial graphene (MEG) on C-face SiC. (1) Heating portion of the experiment and (2) cooling portion of the experiment. Data obtained during desorption are excluded from both plots.

CO_2, the anion will be the bicarbonate ion, HCO_3^- as shown in Equation (1).

In the left panel of Figure 5(a) are the results for the clean graphene/SiC system (after the vacuum annealing process). The system is n-type, with a work function *W(*SiC*)* ~4.1 eV (Ref. 26) and the Fermi energy is pinned by an interface state localized on the C rest atoms of the $(2 \times 2)_C$ surface reconstruction of $(000\bar{1})$ of 6 H-SiC (see Figure 5(c) and Ref. 3). In this case, the Dirac point energy of graphene (the energy of the vertex of the Dirac cone), is lower than the Fermi energy (~−4.46 eV with respect to the vacuum level), in good agreement with the available data.[27] This situation is similar to that of hydrogenated diamond, hence the same charge transfer mechanism that is observed in that case is available to ambient-exposed epitaxial graphene. The chemical potential for the oxygen dissolved in water in contact with the graphene lies between −5.66 eV and −4.83 eV (blue levels in Figure 5(a)) with respect to the vacuum level, depending on the pH value of the solution (0 to 14, respectively).[28] For the solutions with pH = 14, $\mu = -4.83$ eV and the reaction that takes place is $O_2 + 2H_2O + 4e^- = 4OH^-$.[21,29] Spontaneous electron transfer would occur from the graphene to the mildly acidic oxygen/water layer at ambient, mediated by the redox reaction $O_2 + 2H_2O + 4e^- = 2H_2O$.[21,29] Thus, since the Dirac energy of graphene lies near the redox potential of dissolved oxygen, surface electrons will readily transfer from the graphene to the adsorbed water, and the graphene will become p-type. In Figure 5(b), we plot the evolution of the relative position of the Fermi and Dirac energies as a function of the surface charge as obtained in our first principles calculations. The neutrality point is identified with a depletion of $\sim 1 \times 10^{14}$ electrons/cm^2 from the graphene surface. These data correlate directly with the results of our TEP measurements in the monolayer case.

Now it is important to comment on the nonlinear behavior as a function of temperature of both the positive TEP prior to desorption of adsorbed water + oxygen, and the negative TEP after desorption (Figure 6). Interestingly, in contrast with the behavior of TEP, the nonlinear relationship between R and T of ambient exposed sample becomes linear after oxygen desorption. The temperature-dependent electrical conductivity due to screening effects is expected to decrease quadratically.[30] This mechanism in turn produces thermopower that is quadratic in temperature rather than linear, as in the simple Mott formula.[31] Previous works[32,33] on graphene thermopower did not consider temperature dependence due to screening. Moreover, the Mott formula only in the low-temperature limit was considered to calculate the thermopower and so, as a result, the deviations from the Mott formula are observed. This explains the wide variation of measured conductivity.[6–9,12,13]

IV. CONCLUSIONS

In summary, both multilayer and monolayer graphene on C-face SiC show p-type behavior under ambient conditions at 300 K, but become n-type when annealed in high vacuum as observed using both *in-situ* TEP and 4-probe resistance measurements. This implies that the p-type doping is due to ambient-related factors and the natural conductivity state of the epitaxial graphene on C-face SiC is n-type, as expected by work function considerations. It is proposed that an electron exchange between the oxygen electrochemical redox couple in adsorbed water and electronic states in the graphene causes the p-type behavior. The n-type behavior for the vacuum annealed graphene is due to the pinning of the Fermi energy at a state associated with the dangling bonds of the SiC surface.

ACKNOWLEDGMENTS

JLT is grateful for postdoctoral fellowship support from the American Society for Engineering Education. Portions of this work were supported by the Office of Naval Research and by the DARPA-CERA program. MBN wishes to acknowledge partial support from the Office of Basic Energy Sciences, U.S. Department of Energy at Oak Ridge National Laboratory under contract DE-AC05-00OR22725 with UT-Battelle, LLC. GUS acknowledges NSF Grant No. ECCS-0925835.

[1]Y.-M. Lin, C. Dimitrakopoulos, D. B. Farmer, S.-J. Han, Y. Wu, W. Zhu, D. K. Gaskill, J. L. Tedesco, R. L. Myers-Ward, C. R. Eddy Jr., A. Grill, and P. Avouris, "Multicarrier transport in epitaxial multilayer graphene," Appl. Phys. Lett. **97**, 112107 (2010).
[2]R. McKee, F. Walker, M. B. Nardelli, W. A. Shelton, and G. M. Stocks, "The interface phase and the Schottky barrier for a crystalline dielectric on silicon," Science **300** (5626), 1726 (2003).
[3]F. Schedin, A. K. Geim, S. V. Morozov, E. W. Hill, P. Blake, M. I. Katsnelson, and K. S. Novoselov, "Detection of individual gas molecules adsorbed on graphene," Nature Mater. **6**, 652 (2007).
[4]T. O. Wehling *et al.* "Molecular doping in graphene," Nano Lett. **8**(1), 173–177 (2008).
[5]H. E. Romero, P. Joshi, A. K. Gupta, H. R. Gutierrez, M. W. Cole, S. A. Tadigapa, and P. C. Eklund, "Adsorption of ammonia on graphene," Nanotechnology **20**(24), 245501 (2009).
[6]A. K. Geim and K. S. Novoselov, "The rise of graphene," Nature Mater **6**, 183–191 (2007).
[7]K. S. Novoselov *et al.* "Electronic properties of graphene" Phys. Status Solidi B **244**, 4106 (2007).
[8]K. S. Novoselov, A. K. Geim, S. V. Morozov, D. Jiang, M. I. Katsnelson, I. V. Grigorieva, S. V. Dubonos, and A. A. Firsov, "Two-dimensional gas of massless Dirac fermions in graphene," Nature **438**, 7065, 197–200 (2005).
[9]K. S. Novoselov *et al.* "Electric field effect in atomically thin carbon films," Science **306**, 5696, 666–669 (2004).
[10]T. J. Echtermeyer *et al.* "Nonvolatile switching in graphene field-effect devices," IEEE Electron Device Lett. **29**, 952 (2008).
[11]H. Wang, D. Nezich, J. Kong, and T. Palacios, "Graphene frequency multipliers," IEEE Electron Device Lett. **30**, 547 (2009).
[12]W. A. de Heer *et al.* "Epitaxial graphene electronic structure and transport," J. Phys. D: Appl. Phys. **43**, 374007 (2010).
[13]W. A. de Heer *et al.* "Epitaxial graphene," Solid State Commun. **143**, 92–100 (2007).
[14]See supplemental material at http://dx.doi.org/10.1063/1.4725413 for details on C-terminated epitaxial grown graphene sample preparation and application of Electro Static deposition technique for a production of C-terminated epitaxial monolayer graphene; for the simulations, from first principles based on Density Functional Theory, results of TEP and R measurements interpreted in terms of the interplay between bonding and electrochemical reactions at the surface.
[15]T. Jayasekera, B. D. Kong, K. W. Kim, and M. B. Nardelli, "Band engineering and magnetic doping of epitaxial graphene on SiC (0001)," Phys. Rev. Lett. **104**, 146801 (2010).
[16]A. N. Sidorov, M. M. Yasdanpanah, R. Jalilian, P. J. Ouseph, R. W. Cohn, and G. U. Sumanasekera, "Electrostatic deposition of graphene," Nanotechnology **18**, 135301 (2007).
[17]A. N. Sidorov, D. Mudd, G. U. Sumanasekara, P. J. Ouseph, C. S. Jayanthi, and S.-Y. Wu, "Electrostatic deposition of graphene in a gaseous

environment: a deterministic route for synthesizing rolled graphenes?" Nanotechnology **20**, 055611 (2009).
[18]J. L. Tedesco, B. L. VanMil, R. L. Myers-Ward, J. C. Culbertson, G. G. Jernigan, P. M. Campbell, J. M. McCrate, S.A. Kitt, C. R. Eddy Jr., and D. K. Gaskill, ECS Trans. **19**, 137 (2009).
[19]T. Lohmann, K. von Klitzing, and J. H. Smet, "Four-terminal magneto-transport in graphene p-n junctions created by spatially selective doping," Nano Lett. **9**,5, 1973–1979 (2009).
[20]P. L. Levesque *et al*. "Probing charge transfer at surfaces using graphene transistors," Nano Lett. **11**(1), 132–137 (2011).
[21]V. Chakrapani, J. C. Angus, A. B. Anderson, S. D. Wolter, B. R. Stoner, and G. U. Sumanasekera, "Charge transfer equilibria between diamond and an aqueous oxygen electrochemical redox couple," Science **318**, 1424–1430 (2007).
[22]W. Zhang, J. Ristein, and L. Ley, "Hydrogen-terminated diamond electrodes. II. Redox activity," Phys. Rev. E **78**, 4 (2008).
[23]G. U. Sumanasekera, C. K. U. Adu, S. Fang, and P. C. Eklund, "Effects of gas adsorption and collisions on electrical transport in single-walled carbon nanotubes," Phys. Rev. Lett. **85**, 1096 (2000).
[24]V. Derycke, R. Martel, J. Appenzeller, and P. Avouris, "Carbon nanotube inter- and intramolecular logic gates,"Nano Lett. **1**, 453 (2001).
[25]C. M. Aguirre, P. L. Levesque, M. Paillet, F. Lapointe, B. C.St-Antoine, P. Desjardins, and R. Martel, "The role of the oxygen/water redox couple in suppressing electron conduction in field-effect transistor," Adv. Mater. **21**, 3087–3091 (2009).
[26]F. Varchon, R. Feng, J. Hass, X. Li, B. Ngoc Nguyen, C. Naud, P. Mallet, J.-Y. Veuillen, C. Berger, E. H. Conrad, and L. Magaud, "Electronic structure of epitaxial graphene layers on SiC: effects of the substrate," Phys. Rev. Lett. **99**, 126805 (2007).
[27]Y.-J. Yu, Y. Zhao, S. Ryu, L. E. Brus, K. S. Kim, and P. Kim, "Tuning the graphene work function by electric field," Nano Lett. **9**, 10 (2009).
[28]O. Leenaerts, B. Partoens, and F. M. Peeters, "Adsorption of H_2O, NH_3, CO, NO_2, and NO on graphene: A first-principles study," Phys. Rev. B, **77**(12), 125416 (2008).
[29]A. N. Sidorov, A. Sherehiy, R. Jayasinghe, R. Stallard, D. K. Benjamin, Q. Yu, Z. Liu, W. Wu, H. Cao, Y. P. Chen, Z. Jiang, and G. U. Sumanasekera, "Thermoelectric power of graphene as surface charge doping indicator," Appl. Phys. Lett. **99**, 013115 (2011).
[30]E. H. Hwang, E. Rossi, and S. Das Sarma, "Theory of thermopower in two-dimensional graphene," Phys. Rev. B. **80**, 235415 (2009).
[31]J. Small and P. Kim, "Thermopower measurement of individual single walled nanotubes," Microscale Thermophys. Eng. **8**, 1 (2004).
[32]T. Löfwander and M. Fogelström, "Impurity scattering and Mott's formula in graphene," Phys. Rev. B **76**, 193401 (2007).
[33]Y.-J. Yu, Y. Zhao, S. Ryu, L. E. Brus, K. S. Kim, and P. Kim,. "Tuning the graphene work function by electric field," Nano Lett. **9**, 10 (2009).